Proceedings of the ASME 2019
International Offshore Wind Technical Conference
IOWTC2020
October 18-21, 2020, Boston, MA, USA

IOWTC2020-3515

DRAFT: A CFD STUDY FOR FLOATING OFFSHORE WIND TURBINE AERODYNAMICS IN TURBULENT WIND FIELD

Yang Zhou[1], Qing Xiao[1*], Yuanchuan Liu[2], Atilla Incecik[1], Christophe Peyrard[3], Decheng Wan[4], Sunwei Li[5]

[1]Department of Naval Architecture, Ocean and Marine Engineering, University of Strathclyde, Glasgow, G4 0LZ, UK
[2]College of Engineering, Ocean University of China, Qingdao 266100, PR China
[3]Saint-Venant Hydraulics Laboratory (Électricité de France, ENPC, Cerema), Université Paris-Est, 6 quai Watier, 78400 Chatou, France
[4]Computational Marine Hydrodynamics Lab, State Key Laboratory of Ocean Engineering, School of Naval Architecture, Ocean and Civil Engineering, Shanghai Jiao Tong University, Shanghai 200240, China
[5]Division of Ocean Science and Technology, Graduate School at Shenzhen, Tsinghua University, Shenzhen 518055, Guangdong, PR China
*Correspondent: qing.xiao@strath.ac.uk

ABSTRACT

The present study is aimed at investigating the turbulent wind effect on FOWT through the usage of a high-fidelity computational fluid dynamics (CFD) method. This method is believed to resolve the wind field, giving us a more in-depth examination into the aerodynamics of FOWT. The work is built upon our previous studies on the modelling of a coupled aero-hydro-mooring FOWT system under regular wave and uniform wind. In the present study, we replaced the previously uniform wind with a temporal and spatial variable turbulent wind field using a time-varying spectrum. The turbulent wind is generated with Mann's wind turbulence model while the Von Karman wind spectrum is used to represent wind turbulence. The present study shows that when turbulent wind is present, there may be fluctuations of the rotor thrust and power outputs, causing the non-uniform wake region. Despite this, both the dynamic motions and the mooring tensions of the floater are not significantly influenced by the wind turbulence under the present inflow wind conditions.

Keywords: Turbulent wind, Computational Fluid Dynamics (CFD), Floating offshore wind turbine (FOWT)

1. INTRODUCTION

In recent years, the concept of floating offshore wind turbine (FOWT) has been rapidly developing as it is claimed that these FOWT systems can offer a better solution to wind energy compared to onshore wind turbine. Numerical analysis is one of many key tools during the initial FOWT design stage. With the aid of numerical analysis, we are able to predict the aero/hydrodynamic performance of a coupled FOWT system. Nonetheless, the main challenge is how to replicate accurate results under real environmental wave and wind conditions.

Some of the most commonly used methods used to analyse the aerodynamics of a wind turbine include; low-cost Blade Element Method (BEM) and high-fidelity, high-cost Computational Fluid Dynamics (CFD). Due to the fact that CFD allows us to directly solve the fluid flow governing equations, it is able to produce detailed flow variables in both the time and spatial domains so that the transient aerodynamic loading on the tower, the turbine blade, and the wind wake structure can all be well resolved. For a typical FOWT, the operating wind speed and the size of FOWT contribute to channeling the airflow into turbulent regime. This means that CFD modelling for a FOWT must factor in turbulent feature. There are three general approaches for turbulence modelling. These are; Large Eddy Simulation (LES), Direct Numerical Simulation (DNS) and Unsteady Reynolds-Average Navier-Stokes (URANS). Out of these approaches, URANS is considered as a compromising method due to its relatively low computational cost while also having reasonably good predictions for the time-mean variables.

As of right now, most FOWT turbulent analysis simplify the problem by assuming a uniform and constant incoming wind. However, in a non-controlled environment, the real wind field is considered as a stochastic process which varies in both temporal and spatial domains. Because of this, a spectral

method is commonly used so that we can replicate such a turbulent wind field. Here, the given wind spectrum is broken down into a set of turbulent components with various wavenumbers and frequencies. One example of this is the Mann wind turbulence model [1]. This specific model is able to predict a second-order three-dimensional fully turbulence field.

Previous studies into the understanding of turbulent impact on wind turbine began onshore before moving to offshore fixed and floating system. Li et al.[2] utilized the Mann wind turbulence model to analyze a bottom fixed wind turbine aided by CFD code (CFDship-Iowa). The study revealed that turbulence resulted in an increasing of wake diffusion. By using a simple actuator line theory and LES modelling, Troldborg et al.[3] investigated the effect of both uniform and turbulent conditions on a fixed bottom wind turbine. This was done using the Mann wind turbulence model and a simplified wind turbine model. His study reveals that wind turbulence will cause the wake to be unstable. This effect is significantly more prominent in the region closest to the turbine rotor. In addition to this, the study found that the disparity under various wind turbine modelling methods is negligible. The recent research conducted by Li et al.[4] focuses on a floating offshore wind turbine using BEM tool, we are shown that the vertical velocity profile had limited influence on the rotor performance, however, the existence of a turbulent wind field led to a very unstable thrust force and power. Because the wind turbulence will have a significant impact on the wind farm performance, Hugo et al. [5] analyzed the modelling of homogeneous turbulence inflow in turbine wake through utilizing actuator disk(AD) theory and LES modelling. His study showed that the velocity field within the wake region becomes uninform whilst the turbulence kinetic energy increases behind the AD model. This effect is due to the existence of the AD edges. In addition to this, Chivaee et al. [6] performed a study in which he investigated a 2D airfoil under turbulent wind by using LES method and Sub-Grid Scale(SGS) model. His research extended to the wind turbine wake performance under turbulent wind. We can see from his research that the blade tip vortices could be captured accurately under fine mesh resolution. On the other hand, the coarse mesh provides rather poor wake predictions.

The current study investigates the offshore floating wind turbine behavior under the influence of turbulent wind field generated by incoming wind spectrum. The perception is that turbulent wind may have an effect on both the unsteady aerodynamic loading of the wind turbine and hydrodynamic response of floater. This effect may result in the overall performance change of the turbine. The aim is achieved by using our in-house hydro-aero-mooring CFD tool [7-10] with the Mann wind turbulence model. The magnitude and spatial distribution of the turbulence are put in as boundary condition inputs to the CFD solver. The modelling of a FOWT under regular wave condition is then carried out in our numerical wave tank and the aero/hydrodynamic responses are computed before being compared the values predicted by BEM tool.

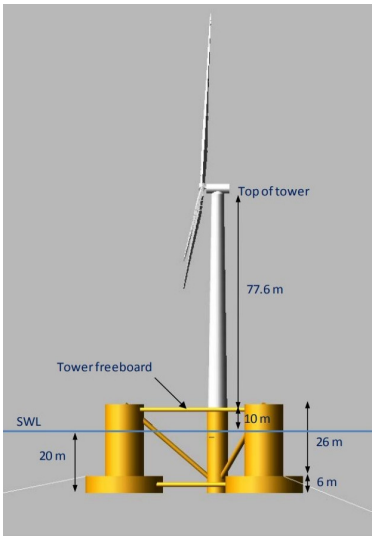

FIGURE 1 GEOMETRY OF THE OC4 SEMI-SUBMERSIBE NREL 5MW FOWT

2. PROBLEM STATEMENT

As shown in Figure 1, the model used in this study is the OC4 semi-submersible NREL 5MW floating offshore wind turbine. In regards to the bottom component, the semi-submersible platform is made up of three offset columns with large heave plate bases, with one center column used to support the wind turbine and several connecting braces which act together to stabilize the floater. The wind turbine subsections include the rotor blades, hub, nacelle and tower. The rotor diameter is 126.0 meters and the hub height is 90 meters above the still water line (SWL).

The present CFD solver is a coupled hydro-aero-mooring solver based on solving the URANS equations by using a finite volume method. This tool has been successfully applied to study FOWT under both regular and focused waves alongside a uniform wind field mentioned in our previous studies [5-8]. Detailed descriptions about the flow solver, mesh moving method, numerical wave generation and the mooring system can be referred to [5-8]. In the following sections, we will provide a brief summary about the main numerical methodology and also focus on the turbulent wind field generation.

3. Mathematical Formulation

3.1 Flow solver

The open source Computational Fluid Dynamics framework OpenFOAM [11] is applied as the flow solver for the duration of the coupled FOWT simulation. The governing continuity and momentum equations for a transient, incompressible flow can be written as,

$$\nabla \cdot U = 0 \tag{1}$$

$$\frac{\partial \rho U}{\partial t} + \nabla \cdot \left(\rho(U - U_g)U\right) = -\nabla P_d - g \cdot x \nabla \rho + \nabla\left(\mu_{eff} \nabla \mathrm{U}\right) + (\nabla \mathrm{U}) \cdot \mu_{eff} + f_\sigma \tag{2}$$

Where U and U_g represent the velocity of the flow field and grid nodes in Cartesian coordinates, ρ refers to the mixed

density of water and air, g denotes the gravity acceleration and P_d is the dynamic pressure. We can use $\mu_{eff} = \rho\ (v + v_t)$ to calculate the effective dynamic viscosity, in which v and v_t are the kinematic and eddy viscosity respectively and f_σ is the surface tension..

The k-ω SST turbulent model is used in order to deal with a high Reynolds number of wind. This may reach values as high as Re=10^7 for a typical wind turbine. As indicated by previous studies, the k-ω SST turbulence model [12] is made up from a combination of the standard k-ω model with the k-ε model. This design shows its strengths in adverse pressure gradients and predicting separating flow. To make capturing the air-water free surface possible, the Volume of Fluid (VOF) method [13] is applied, in which the free surface is represented by the volume fraction. To generate regular waves in our numerical wave tank, an open-source toolbox "waves2Foam" [14] is used. The relaxation zone technique is adopted to provide better wave quality whilst also avoiding wave reflection in the absorbing zones. This technique is applied at both inlet and outlet boundaries in the numerical wave tank.

3.2 Mooring line modelling

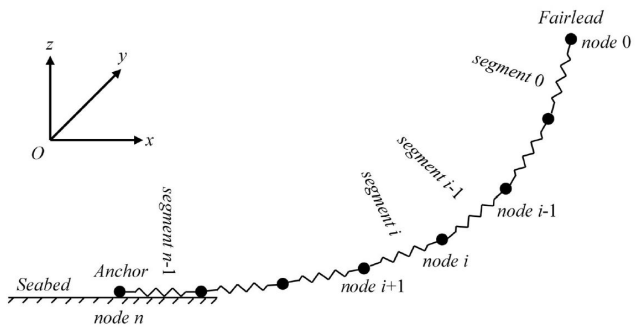

FIGURE 2 3D LUMPED MASS DYNAMIC MOORING LINE MODELLING

The mooring lines are not directly simulated in the CFD computational domain. Instead, the tension loads of mooring lines are added as constraints on the patches of the floater onto the computational mesh. In order to capture the tension loads subjected to mooring lines, a 3D-lumped mass method is adopted to perform the dynamic mooring line behavior. The sketch of dynamic mooring line modelling is shown in Figure 2. The mooring line is discretized into several segments[15],. All the segments have to satisfy the equilibrium equations both in the horizontal and vertical directions as shown below;

$$T_{x(i+1)} = T_{xi} \tag{3}$$

$$T_{z(i+1)} = T_{zi} - w_i l_i \tag{4}$$

Where T_x and T_z refers to the tension force in horizontal and vertical components at the two adjacent nodes (node i and node i+1) connected by segment i. $w_i l_i$ represents the segment weight in water. In addition to this, each segment has to consider the dynamic effects in a lumped mass model.

3.3 Turbulent wind modelling

To solve the problem of turbulent wind modelling, the Mann [1] method is implemented into the current flow solver. As we can see in [7], the Mann wind turbulence box is based off the construction of a velocity-spectrum tensor (ϕ_{ij}) of a neutral atmospheric boundary layer (ABL). The turbulence field is then reproduced with second-order statistics derived from two things, either from the covariance tensor or from its Fourier transform. Most of the time, they are relevant to the spectral tensor (i.e. Von Karman tensor). However, the stochastic velocity field $u(x)$ does not have a direct Fourier transform as it is unable to be integrated over the space. Mann's velocity field can be represented in terms of a generalized Fourier-Stieltjes integral

$$\mathrm{u(x)} = \int \mathrm{e^{i\kappa\cdot x} d\mathbf{Z}(\kappa)} \tag{5}$$

In which κ represents the wavenumber vector and the integration of κ covers all the wavenumber space which makes up the velocity field. $\mathbf{Z}(\kappa)$ refers to a complex orthogonal stochastic process. This process can then be used to calculate the velocity-spectrum tensor ϕ_{ij}

$$\phi(x)_{ij} d\kappa_1 d\kappa_2 d\kappa_3 = \langle d\mathbf{Z_i^*}(\kappa) d\mathbf{Z_j}(\kappa) \rangle \tag{6}$$

Where * stands for the conjugate and $\langle * \rangle$ represents averaging. Because the velocity-spectrum tensor ϕ_{ij} is related

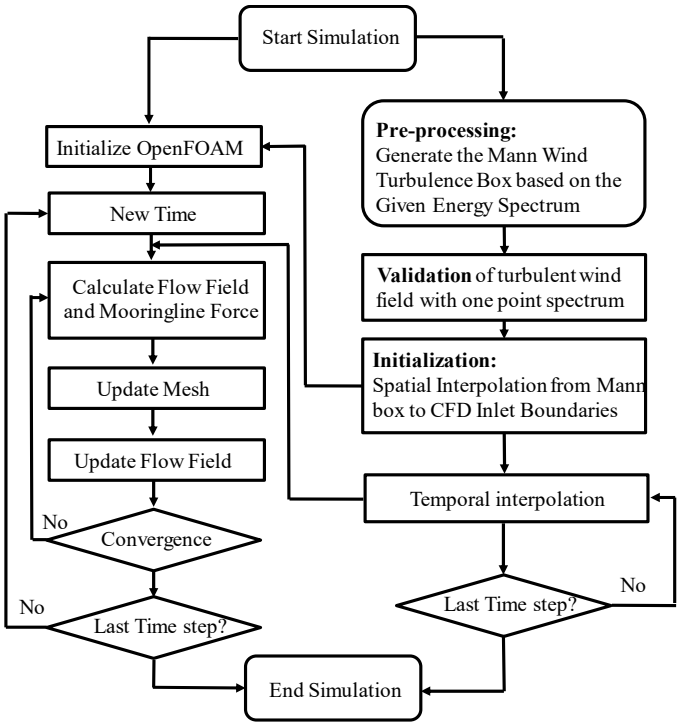

FIGURE 3 LAYOUT OF THE IMPLEMENTATION OF MANN WIND TURBULENCE TO OPENFOAM

to its covariance three-dimensional energy spectrum, if the flow is thought to be incompressible, the spectral tensor can be given by the formula

$$\phi_{ij}(\kappa) = \frac{E(\kappa)}{4\pi\kappa^4}(\delta_{ij}\kappa^2 - \kappa_i\kappa_j) \quad (7)$$

Due to the fact that Von Karman spectrum[16] is one of the recommended energy spectrums in IEC standard, it is selected in the present study. This is given as:

$$E(\kappa) = \alpha\varepsilon^{2/3}L^{5/3}\frac{L^4\kappa^4}{(1+L^2\kappa^2)^{17/6}} \quad (8)$$

Where α is the Kolmogorov constant, ε is the rate of dissipation of turbulent kinetic energy (TKE) and L represents a length scale. As it is currently impossible to measure the energy spectrum experimentally, we must utilize one-dimensional spectra which is derived after following the relationship with three-dimensional spectrum [17]. The one-dimensional Von Karman spectrum can be expressed as follows, for the spectrum relating to longitudinal direction

$$F_1(\kappa_1) = \frac{9}{55}\alpha\varepsilon^{2/3}L^{5/3}\frac{1}{(1+L^2\kappa_1^2)^{5/6}} \quad (9)$$

For the spectrum of transversal direction (i=2,3),

$$F_i(\kappa_1) = \frac{3}{110}\alpha\varepsilon^{2/3}L^{5/3}\frac{3+8L^2\kappa_1^2}{(1+L^2\kappa_1^2)^{11/6}} \quad (i = 2,3) \quad (10)$$

3.3 Implementation wind turbulence to flow solver

The Mann wind turbulence method described above has been built into our coupled hydro-aero-mooring CFD solver. The structure in which it was implemented into the simulation is displayed in Figure 3. We can see it is carried out in three steps. Firstly, the homogeneous isotropic turbulence wind field has to be generated. Fast Fourier transform is utilized to compute the velocity field with the given one-dimensional spectra, i.e., equations (7) & (8). After doing so, we are able to generate a three-dimensional field with this data. Taylor's frozen hypothesis is used to transfer time series into space series. Based on this, velocities are extracted from different sections of the Mann wind turbulence box, and various time-domain results can be obtained along a transversal plane in Mann box. The relationship between a longitudinal dimension and time is given as,

$$x = L_1 - U_{mean}t \quad (11)$$

Where L_1 is the longitudinal dimension of the Mann wind turbulence box and U_{mean} equals the mean wind velocity at a

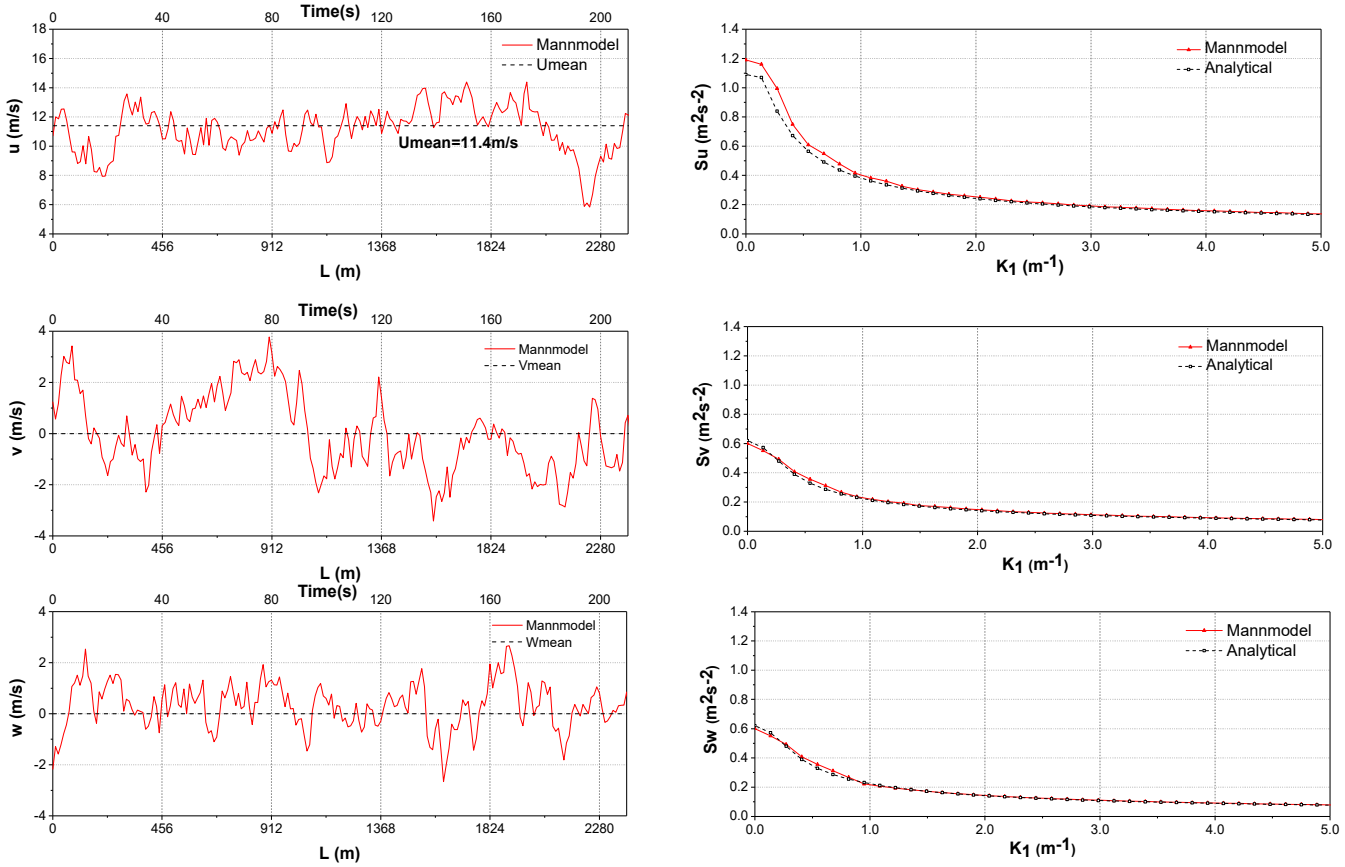

FIGURE 4 MANN WIND TURBULENCE BOX VALIDATION LEFT: VELOCITY DISTRIBUTION ALONG THREE DIRECTIONS AT HUB LOCATION; RIGHT: ONE-DIMENSIONAL VELOCITY SPECTRA FOR EACH VELOCITY COMPONENT COMPUTED FROM MANN WIND TURBULENCE BOX

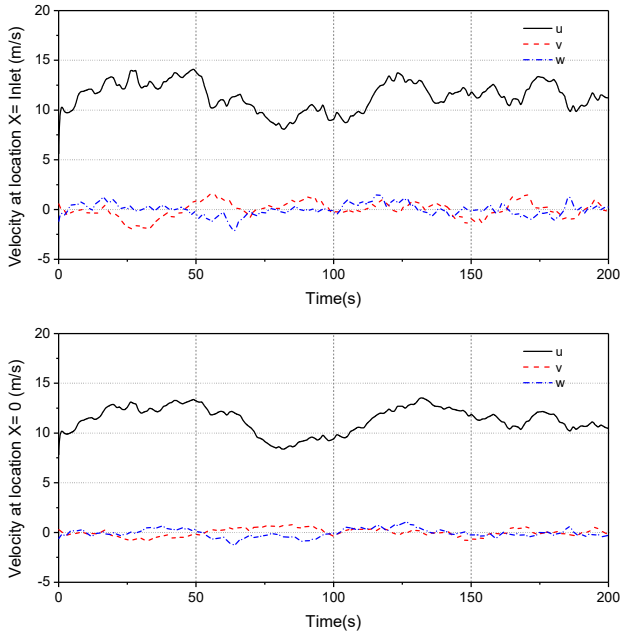

FIGURE 5 TIME HISTORY OF VELOCITIES AT HUB HEIGHT IN INLET BOUNDARY AND ROTOR PLANE POSITIONS IN CFD CALCULATION WITHOUT FOWT STRUCTURE

specific turbine hub height. The generated turbulence wind field has to be evaluated against the given wind power spectrum first before they are inputted as the wind turbulent boundary conditions onto the CFD computational domain. Because the CFD mesh is finer than the discretized wind field in Mann wind turbulence box, a trilinear interpolation is required. This allows us to obtain all relevant turbulent velocities at the CFD mesh along the inlet boundary. It was also taken into account that as the unsteady CFD modelling time step is significantly shorter compared to the time step used for the turbulent wind field generation, a similar time interpolation is also required.

4. Verification and Validation

4.1 Validation of the implementation for Mann wind turbulence model

The study conducted below validates the generation of the turbulence wind field based on Mann's algorithm. Firstly, the results are compared against the one-point velocity spectra, previously defined in Equations (5) and (6). The mean velocity is established as the rated wind speed at 11.4m/s of a NREL 5MW wind turbine. The Mann wind turbulence box domain is defined as $Lx \times Ly \times Lz = 2400m \times 500m \times 300m$. The length increment of the domain cells is set to $10m$ in both the longitudinal and transversal directions. We can see the velocity distribution at the turbine hub (i.e. Y=0m and Z=90m) along the three directions displayed in Figure 4 along with the spectra produced as a result of the Mann model. The velocities vary throughout the entirety of the spatial domain, with a specific fluctuation of g $\pm 6m/s$, $\pm 4m/s$, $\pm 3m/s$ for longitudinal

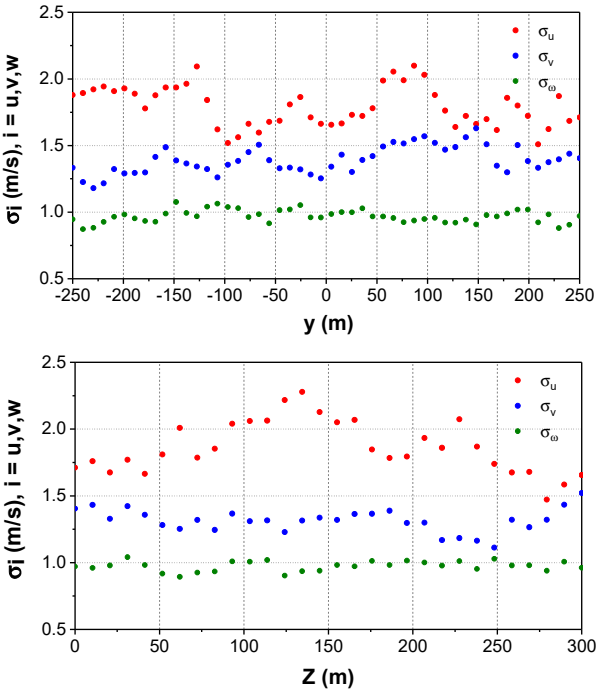

FIGURE 6 STANDARD DEVIATION OF FLOW FIELD FOR XOY & XOZ PLANE.

and transversal velocity respectively. Figure 4 shows the comparison between the theoretical transversal velocity one-point velocity spectra against the spectrum obtained from the Mann model. The values Su, Sv and Sw represent the spectrum calculated on the u, v and w velocities respectively. Figure 5 presents the velocities at various axial positions in CFD domain without the FOWT structure where the decay of turbulence could be found due to to the nature of URANS numerical methods.

Figures 6 shows the standard deviation of the velocity distribution along the XoY and XoZ planes. The standard deviation in x, y and z velocity is set as 2.0m/s, 1.4m/s, 1.0m/s respectively. These values satisfy the IEC standard of. $\sigma_2 \geq 0.7\sigma_1, \sigma_3 \geq 0.5\sigma_1$. As we can see from the the Figure 6, the standard deviation calculated from the Mann box remains consistent with the given one point spectrum. Despite this, the turbulence intensity calculated to be 0.23 is higher than the IEC standard of. TI=0.12 for axial velocity. A plausible explanation for this disparity may be a result of the inclusion of the URANS method to solve the flow equations. This may lead to an inevitable dissipation of turbulence in time and space., We can use Larsen[18] recommended turbulence scaling factor in order to minimize the turbulent decay effect. We can estimate a value by taking the actual fluctuation in the Mann box and also the target turbulence standard deviation $\sigma_{target} = \sigma_{iso}/0.55$ based on the reference turbulence intensity.

4.2 Validation of dynamic response and aerodynamic performance of FOWT

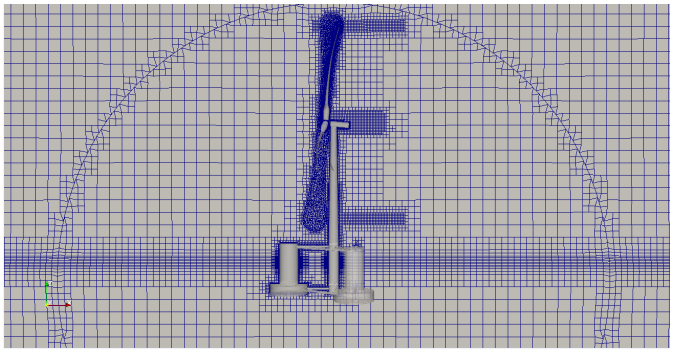

FIGURE 7 COPMUTATIONAL MESH OF OC4 NREL 5MW FOWT

The present hydro-aero-mooring CFD solver has been validated through several OC4 Semi-submersible NREL-5MW FOWT studies which can be seen in our previous papers [7] . These verifications cover the hydrodynamic responses of the floating structure, the aerodynamic performance of the wind turbine and the tension loads of the mooring lines under both regular and focused wave with a uniform wind field.

The mesh sensitivity study on the topic of FOWT modelling was carried out by using three different sets of mesh in our previous studies [7]. The hydrodynamics responses, the aerodynamic thrust and torque were compared and analyzed. The results showed that the disparity is acceptable under different meshes.

5. NUMERICAL SETUP

5.1 Computational domain and boundary conditions

As was previously mentioned, the dimensions of CFD domain are different than those from the Mann turbulence box. This is summarized in Table 1. As seen, the X and Y dimensions of the Mann turbulence box are larger than those of CFD referred by some studies [3-6]. This allows us to achieve the spatial interpolation of the turbulent velocity field originally generated in the Mann box. However, the Z dimension of the Mann turbulence box is smaller than that of CFD domain. This is due to the inclusion of the water wave phase in CFD modelling, e.g. a water depth of 200m is included.

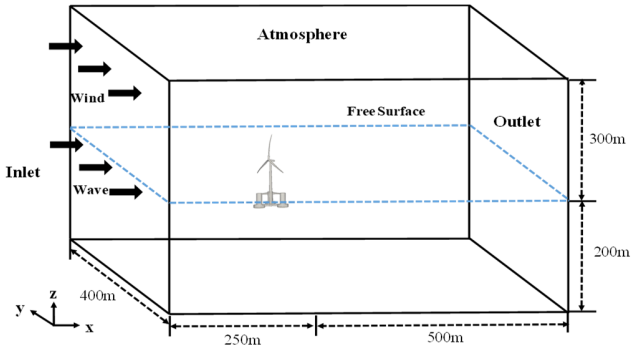

FIGURE 8 SKETCH OF CFD COMPUTATIONAL DOMAIN OF FOWT MODELLING

TABLE 1: MAIN PARAMETERS OF THE COMPUTATIONAL DOMAIN OF CFD AND MANN TURBULENCE BOX, D REFERS TO THE SPACING OF OFFSET COLUMNS OF PLATFORM (50M)

	OpenFOAM (CFD)	Mann Turbulence Box
Domain Size	$750m \times 400m \times 500m$ $15D \times 8D \times 10D$	$2400m \times 500m \times 300m$ $48D \times 10D \times 6D$
Domain Grid	$4899720\ cells$	$240 \times 50 \times 30\ cells$

A built-in arbitrary mesh interface (AMI) method in OpenFOAM can be used to analyse the motion of OC4 semi-submersible NREL 5MW FOWT. Figure 7 shows the partial mesh on the structure and AMI surface of the entire computational domain. We can see that a built-in tool (snappyHexMesh) has been adopted. The total mesh for the present CFD computation is 4899720. Grid refinement is applied near the free surface and the FOWT. On top of this, eight layers of boundary layer mesh with the first layer grid thickness of 0.4mm and a progression rate of 1.1 is added. This is to ensure the y+ value is in the range of [30,300] and wall functions are adopted for near wall treatments in SST k-w turbulence model. In addition, relaxation zones are then set to achieve a better wave quality and also to reduce the wave reflection. The length of these zones are defined as follows, i.e., inlet relaxation zones: $-250 < x < -50m$, outlet relaxation zones: $50 < x < 500m$.

The sketch of the boundary conditions of CFD domain is shown in Figure 8. At the inlet boundary (where x=0), the velocity is defined as the prescribed incident regular wave and turbulent or uniform wind speed without wind shear. The turbulent wind parameters are described previously in Section 4.1and the uniform wind velocity is set as the mean velocity, i.e., 11.4m/s. The regular wave height is H=7.58m and the wave period is T=12.1s. This is also the standard North Sea state. The rate ω, is estimated by using Equations (10 and 11) and can be calculated based on the following equations (Tian's research [19]), where I is the turbulence intensity and $\frac{\mu_t}{\mu}$ representing the viscosity ratio.

$$\kappa = \ 1.5(UI)^2 \tag{10}$$

$$\omega = \frac{\rho\kappa}{\mu}\frac{\mu_t}{\mu}^{-1} \tag{11}$$

The gradient of velocity is represented by κ and ω. This value is set to zero at the outlet boundary (x=750m). The front and back boundaries (y=±200m) are imposed symmetrically and the top and bottom boundaries (z=+300m and -200m) are set as the zero gradient in all terms. The non-slip wall boundary with zero pressure gradient is defined on the patches of the FOWT.

The time step can be set to as small as 0.001s of the FOWT simulation under either uniform wind or turbulent wind. The computational cost under both wind types is negligable, i.e., It takes 200 cores to run in parallel for 580 hours (nearly 24 days) to simulate a result of 200 seconds.

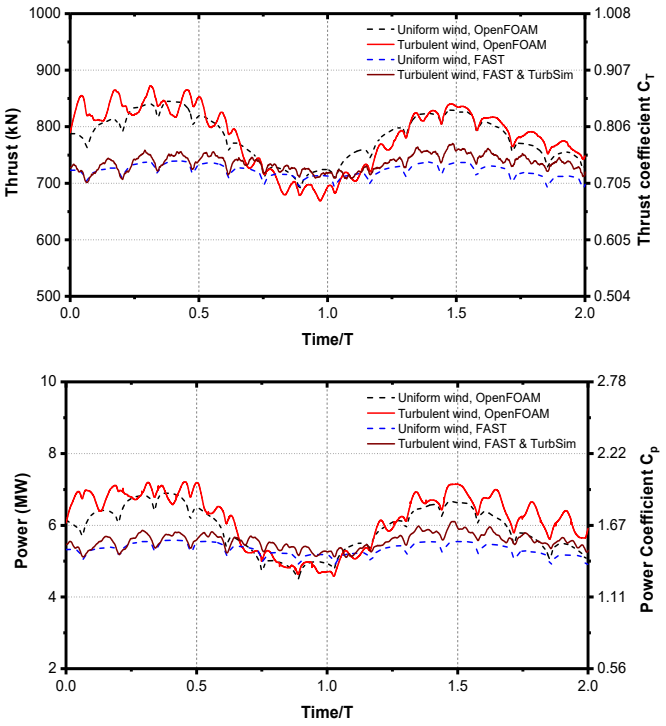

FIGURE 9 THURST AND POWER OUTPUPTS OF FOWT UNDER UNIFORM FLOW AND TURBLENT FLOW WITH U (UMEAN) 11.4M/S

6. RESULTS

6.1 Aerodynamic performance

Figure 9 shows the time history of rotor thrust and power predictions under two sampled regular wave periods (72s-96s) while subject to both uniform and turbulent flow conditions. They are compared to the BEM results provided by using NREL FAST V8 and TurbSimV1.06. The instantaneous time is non-dimensionalized by the wave period (T). The thrust force of CFD can be estimated using the sum of aerodynamic force exerted on three blades and the rotor along x direction. The power is calculated by multiplying the rotor torque with the angular velocity of the blades. Non-dimensionally, the thrust coefficient is can be worked out using the formula $C_T = Thrust/0.5\rho RU^2$ while the power coefficient is estimated by using $C_p = Power/0.5\rho RU^3$, where R refers to the rotor radius and U represents the wind speed. Under the condition of uniform wind, the wind speed is set to 11.4m/s for both CFD and BEM without the wind shear. Under the influence of a turbulent flow, the wind energy spectrum and Von Karman wind spectrum, are also set to the same values for both methods.

We can see from Figure 9 that the values for both CFD and NREL FAST show a similar trend in terms of the rotor thrust force and the power output of the wind turbine. A few local minimum values along the thrust force and power curve are found simultaneously, i.e., at the time instances 0.05T, 0.19T, 0.33T, 0.47T etc. These sudden dips range from 5-7% of the average thrust force and power. They are found occur at every 1/3 rotation of the wind turbine when the blades have rotated in front of the tower.

The comparison between uniform and turbulent wind field suggests that the existence of turbulence increases the peak of thrust and power when compared with uniform wind. In addition, CFD predicts a larger magnitude of fluctuation than FAST results, however, there is also a relatively low frequency variation in the thrust and power. This may be directly caused by the turbulent decay associated with the URANS CFD modelling in this work.

In order to have a better understanding of the effect that turbulent wind has on the aerodynamic performance of wind turbine, a statistical analysis has to be carried out. The results of this analysis is summarized in Table 2 for the peak and time-mean parameters. Time-mean thrust results from CFD indicate that even though the mean magnitude is almost identical for uniform (783.7KN) and turbulent wind (781.3KN), the standard deviation of turbulent (53.1KN) is reasonably higher than uniform wind (39.7KN). This is also reflected in the results of the NREL FAST analysis. In addition, the difference of peak thrust and power between uniform and turbulent wind is

TABLE 2: STATISTICS OF THURST AND POWER OF WIND TURBINE UNDER UNIRFORM WIND (U=11.4M/S) AND TURBULENT WIND (UMEAN=11.4M/S)

		CFD		NREL FAST	
		Turbulent wind	Uniform wind	Turbulent wind	Uniform wind
Thrust (KN)	Max/Diff	872.2 (3.05%)	846.4 (0.00%)	770.4 (4.13%)	739.8 (0.00%)
	Min/Diff	668.6 (−3.14%)	690.3 (0.00%)	701.1 (1.14%)	693.2 (0.00%)
	Mean/Diff	783.7 (0.31%)	781.3 (0.00%)	735.1 (1.65%)	723.2 (0.00%)
	σ	53.1	39.7	14.3	10.2
Power (MW)	Max/Diff	7.21 (4.49%)	6.90 (0.00%)	6.11 (9.49%)	5.58 (0.00%)
	Min/Diff	4.58 (1.70%)	4.50 (0.00%)	5.10 (4.08%)	4.90 (0.00%)
	Mean/Diff	6.16 (4.76%)	5.88 (0.00%)	5.54 (3.74%)	5.34 (0.00%)
	σ	0.76	0.63	0.21	0.15

slightly larger than their time-mean values.

It should be noted however, that the thrust and power are dominantly controlled by the wind speed upstream of the rotor blades, therefore, the large time-variable peak thrust with turbulence found in the study does not necessarily indicate the time-mean thrust is larger in the absence of turbulence.

6.2 Impact on the flow field and wake region under turbulent wind

Figure 10 shows the instantaneous velocity contour on a horizontal XoY plane when Z=90m both with and without turbulence at a time instant of t=0.9T. The vorticity plots rendered as the ISO surfaces of Q is also set to 1, colored by the axial velocity. When we compare the two Figures, we can see a typical spatial variation and that there are obvious differences between the two conditions. When turbulence is present, the wind field upstream of the turbine shows a lower speed regime than that of when turbulence is absent. Referring to Figure 9, where the thrust time sequence is plotted, we can see at t=0.9T, the instantaneous thrust in the presence of turbulence is less than the value measured when turbulence is absent. The low speed regime upstream of turbine can be held responsible for why the thrust is smaller. Such an effect also causes the wake downstream of the turbine to appear more unsteady and non-uniform, the turbulent diffusive nature leads further to the weaker vortices forming between the hub and blades. This phenomena was also observed in the works of Li et al. [2].

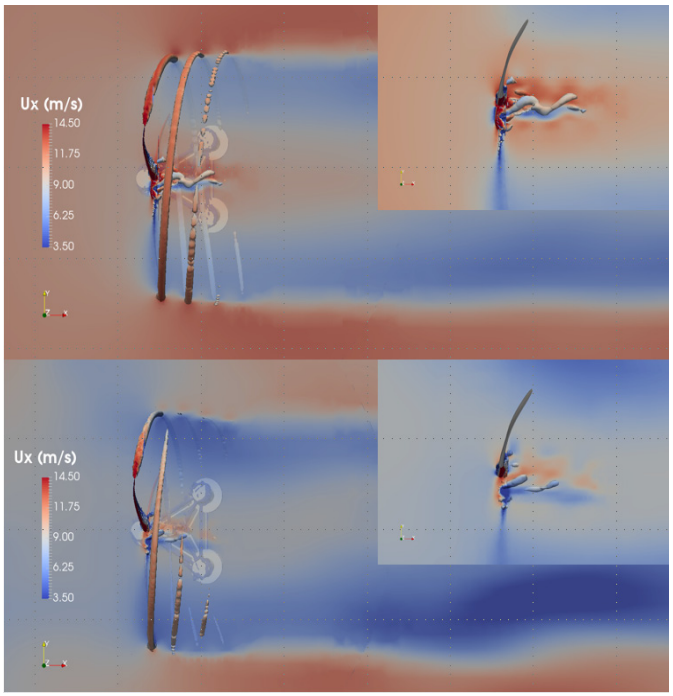

FIGURE 10: INSTANTANEOUS FLOW FIELD IN A HORIZONTAL SECTIONAL PLANE COLORED BY AXIAL VELOCITY LOCATED AT THE HUB HEIGHT (Z=90M) AT INSTANT TIME OF 0.9T., TOP: UNFIROM WIND, BOTTOM: TURBULENT WIND

Figure 11 plots the vertical section view of the flow field at the mid-plane (XoZ) of computational domain for the results obtained when turbulence is present and when it is absent at two time instants, i.e., 0.9T & 1.4T, where the free surface of water-air is also included. We can see that the airflow is significantly affected by the water wave propagation. This is indicated by the reduced air velocity above both the wave crests and troughs near the free surface. Also we can see that the appearance of the turbine tower and semi-submersible platform has a significant impact on the wind flow field near the free surface. Similar to the findings from Figure 10, the turbine wake at XoZ plane becomes more non-uniform when turbulence is present than when turbulence is absent. The plots in Figure 12 for the instantaneous turbulence intensity (TI) contour at Y= 0m XoZ plane show that there is large variation of TI. This variation can be seen not just around the rotor, but also at the tip of the turbine blade.

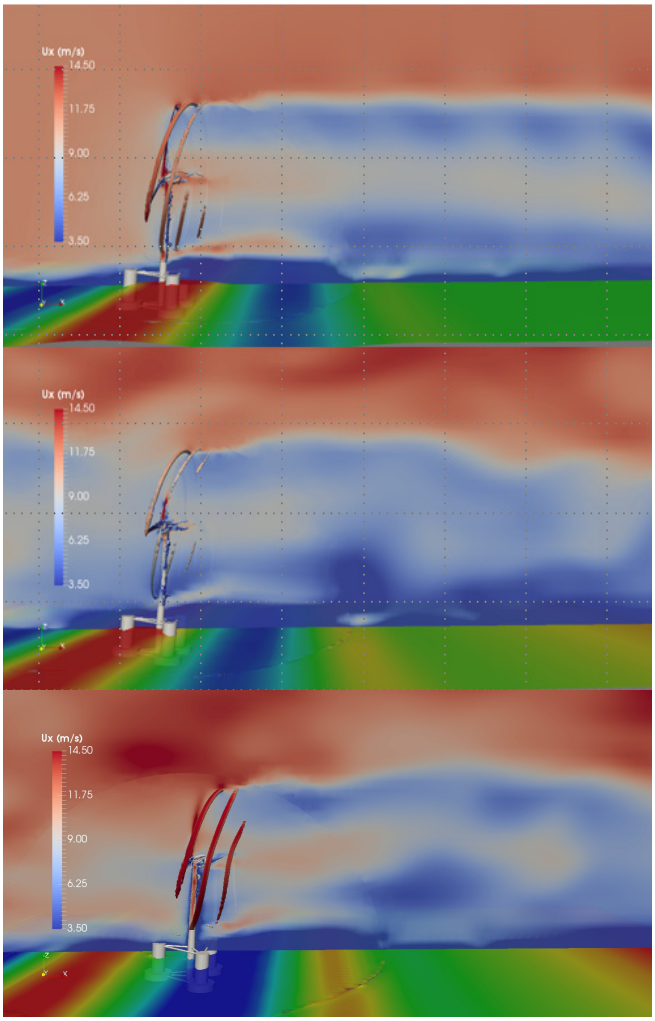

FIGURE 11: INSTANTANEOUS FLOW FIELD IN A SECTIONAL VERTICAL MID-PLANE (Y=0M) COLORED BY AXIAL VELOCITY: TOP: UNFIROM WIND AT INSTANT TIME OF 0.9T, BOTTOM: TURBULENT WIND AT INSTANT TIME OF 0.9T & 1.4T

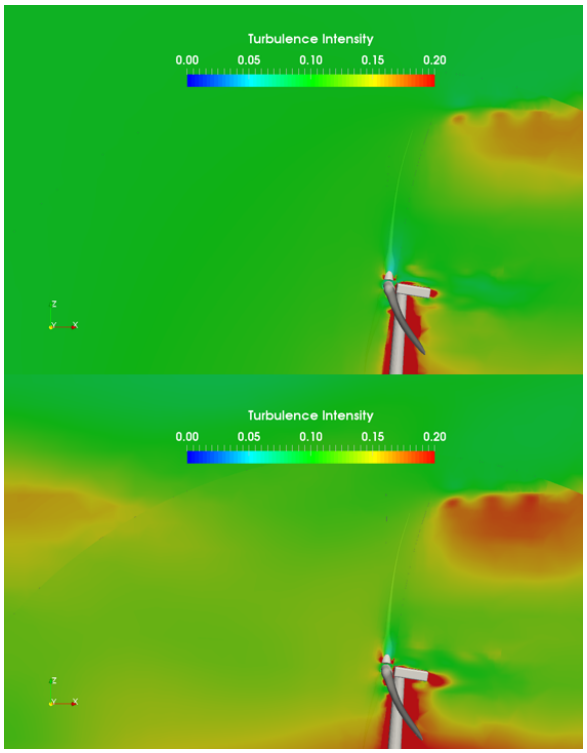

FIGURE 12: TURBULENCE INTENSITY DISTRIBUTION ALONG THE XOZ PLANE (Y=0) AT INSTANT TIME OF 0.9T TOP: UNIFORM WIND, BOTTOM: TURBULENT WIND

Figure 13 shows the air flow field contours at four different span-wise sections of blade-1, i.e. the blade with an azimuth angle of 0 degrees in Figure 1, colored by the axial velocity. The sectional location can be represented by the ratio of r/R, when r/R=0 indicates the slice of blade root and r/R=100% refers to the section at the tip of the blade. As no aero-elastic feature of the blade is taken into account in this simulation, the

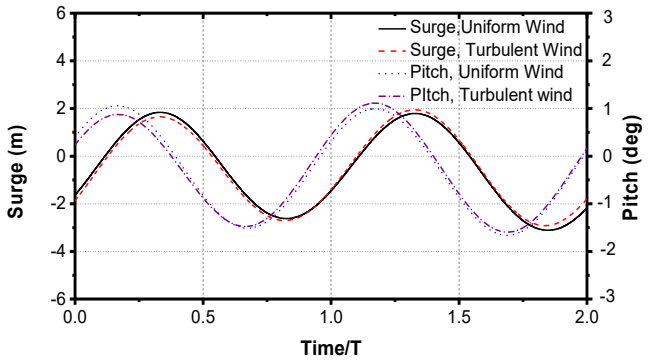

FIGURE 14: SURGE AND PITCH MOTION UNDER IDENTICAL REGULAR WAVES (H=7.58M, T=12.1S) AND UNIFORM WIND (U=11.4M/S)/TURBULENT WIND (UMEAN=11.4M/S)

Angle of Attack (AoA) of the different slices of the blade is constant (reference value could be found in NREL reports[20]). For both uniform and turbulence wind, Figure 13 shows that the flow separation occurs at 1/3-1/2 chord length from the foil leading edge. This value starts along the top surface of the foil, and extends to the trailing edge. The recirculation regime associated with a reversed pressure and negative velocity becomes more profound when the flow moves from the foil root to the tip, with an increasing value of r/R.

In summary, as a high-fidelity analysis tool for turbine aerodynamic study under turbulent wind condition, CFD shows several advantages. These include; capturing the detailed flow field near the wind turbine blades, the wake region and the span-wisely blades sectional-views which can not be achieved by using the BEM tool.

6.3 Hydrodynamic response

Excluding the aforementioned details regarding wind turbine aerodynamics, the involvement of turbulent wind may also have an effect on the FOWT hydrodynamic response.

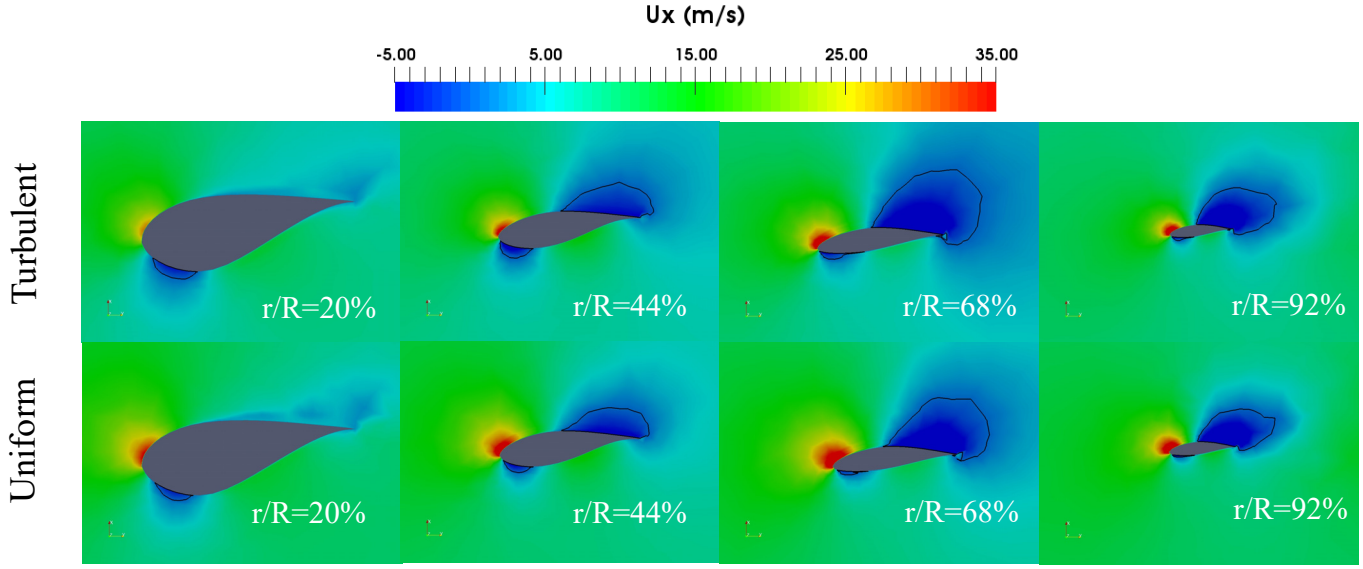

FIGURE 13: INSTANTANEOUS FLOW FIELD CONTOURED BY AXIAL VELOCITY ALONG DIFFERENT BLADE SECTIONAL VIEWS AT 0.9T

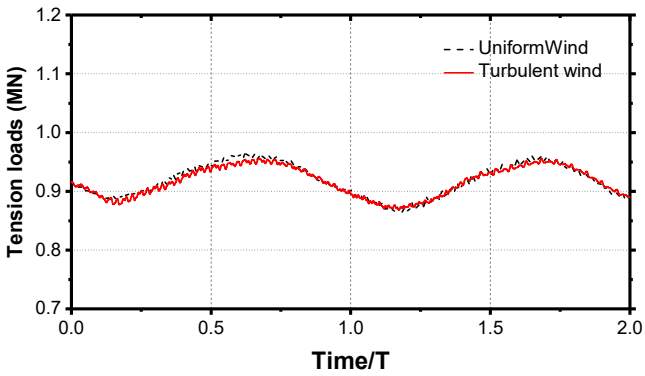

FIGURE 15 TENSION LOADS OF ONE MOORING LINE (CONNECTED WITH THE LARBOARD COLUMN) UNDER REGULAR WAVES (H=7.58M,T=12.1S) AND UNIFORM WIND (U=11.4M/S) OR TURBULENT WIND (UMEAN=11.4M/S)

Figure 14 illustrates the time sequence of the surge and pitch modes under uniform and turbulent wind conditions within two sampled regular wave periods. We can see from the figures, the response amplitude/RAO is nearly identical regardless of whether the wind is uniform or turbulent. This suggests that the turbulent wind has a negligible effect on the dynamic response of the FOWT substructure. Adding onto this, in contrast to the appearance of fluctuation of both thrust and power curves in Figure 9, here, there is no observable fluctuation on the curve of the floater, indicating that the excitation of the incident wave force and the tension loads of mooring lines are the dominant factors alongside the dynamic motion responses of FOWT as well as the unsteady tension loading as shown in Figure 15.

7. CONCLUSION

The paper investigated an OC4 Semi-submersible NREL 5MW floating offshore wind turbine under both uniform and turbulent wind conditions. It began with the generation of the wind turbulence based on the Mann wind turbulence model, followed by a validation of the wind spectrum in comparison with the theoretical wind spectrum. The study was carried on to the examinate the influence of wind turbulence on the aerodynamics performance of the turbine and the dynamic responses of the floater. The comparison between turbulent wind and uniform wind suggests that the presence of wind turbulence caused the rotor thrust to fluctuate and thus affecting the power output of turbine. However, the floater motion responses, including the tension loads of the mooring line, are not greatly influenced by the wind turbulence.

ACKNOWLEDGEMENTS

Results were obtained using the Cirrus UK National Tier-2 HPC Service at EPCC (http://www.cirrus.ac.uk) funded by the University of Edinburgh and EPSRC (EP/P020267/1). Also, Results were obtained using the ARCHIE-WeSt High-Performance Computer (www.archie-west.ac.uk) based at the University of Strathclyde. The first author would like to thank China Scholarship Council (CSC) for financial support during his Ph.D. study in the UK.

REFERENCES

[1] Mann, J., 1994, "The spatial structure of neutral atmospheric surface-layer turbulence," Journal of fluid mechanics, 273, pp. 141-168.
[2] Li, Y., Castro, A., Sinokrot, T., Prescott, W., and Carrica, P., 2015, "Coupled multi-body dynamics and CFD for wind turbine simulation including explicit wind turbulence," Renewable Energy, 76, pp. 338-361.
[3] Troldborg, N., 2009, "Actuator line modeling of wind turbine wakes."
[4] Li, L., Liu, Y., Yuan, Z., and Gao, Y., 2018, "Wind field effect on the power generation and aerodynamic performance of offshore floating wind turbines," Energy, 157, pp. 379-390.
[5] Olivares Espinosa, H., 2017, "Turbulence modelling in wind turbine wakes," École de technologie supérieure.
[6] Chivaee, H. S., 2014, Large eddy simulation of turbulent flows in wind energy, DTU Wind Energy.
[7] Liu, Y., Xiao, Q., Incecik, A., Peyrard, C., and Wan, D., 2017, "Establishing a fully coupled CFD analysis tool for floating offshore wind turbines," Renewable Energy, 112, pp. 280-301.
[8] Liu, Y., Xiao, Q., Incecik, A., and Peyrard, C., 2018, "Aeroelastic analysis of a floating offshore wind turbine in platform-induced surge motion using a fully coupled CFD-MBD method," Wind Energy.
[9] Liu, Y., 2018, "A CFD study of fluid-structure interaction problems for floating offshore wind turbines," PhD thesis, University of Strathclyde.
[10] Zhou, Y., Xiao, Q., Liu, Y., Incecik, A., Peyrard, C., Li, S., and Pan, G., 2019, "Numerical modelling of dynamic responses of a floating offshore wind turbine subject to focused waves," Energies, 12(18), p. 3482.
[11] OpenFOAM, 2019, "The OpenFOAM Foundation Website."
[12] Menter, F., "Zonal two equation kw turbulence models for aerodynamic flows," Proc. 23rd fluid dynamics, plasmadynamics, and lasers conference, p. 2906.
[13] Hirt, C. W., and Nichols, B. D., 1981, "Volume of fluid (VOF) method for the dynamics of free boundaries," Journal of computational physics, 39(1), pp. 201-225.
[14] Jacobsen, N. G., Fuhrman, D.R., Fredse,J., 2012, "A wave generation toolbox for the open-source libradry: OpenFOAM," Internationa Journal Numerical Methods in Fluid, 70, pp. 1073-1088.
[15] Fan, T., Qiao, D., and Ou, J., "Optimized design of equivalent truncated mooring system based on similarity of static and damping characteristics," Proc. The Twenty-second International Offshore and Polar Engineering Conference, International Society of Offshore and Polar Engineers.
[16] Von Karman, T., 1948, "Progress in the statistical theory of turbulence," Proceedings of the National Academy of Sciences of the United States of America, 34(11), p. 530.
[17] Pope, S. B., 2001, "Turbulent flows," IOP Publishing.

[18] Larsen, T., 2011, "Turbulence for the IEA annex 30 OC4 project," IEA: Paris, France.
[19] Tian, X., Ong, M. C., Yang, J., and Myrhaug, D., 2013, "Unsteady RANS simulations of flow around rectangular cylinders with different aspect ratios," Ocean Engineering, 58, pp. 208-216.
[20] Jonkman, J., Butterfield, S., Musial, W., and Scott, G., 2009, "Definition of a 5-MW reference wind turbine for offshore system development," National Renewable Energy Lab.(NREL), Golden, CO (United States).